through the geological record, and time-series data from a broadly equivalent South African core are available (along with data tables) as supporting material on *Science* Online.
6. R. E. Summons, L. L. Jahnke, J. M. Hope, G. A. Logan, *Nature* **400**, 554 (1999).
7. J. J. Brocks, G. A. Logan, R. Buick, R. E. Summons, *Science* **285**, 1033 (1999).
8. R. E. Summons *et al.*, *Philos. Trans. R. Soc. London Ser. B* **361**, 951 (2006).
9. A. D. Anbar *et al.*, *Science* **317**, 1903 (2007).
10. K. A. Baublys, S. D. Golding, E. Young, B. S. Kamber, *Rapid Commun. Mass Spectrom.* **18**, 2765 (2004).
11. S. Ono *et al.*, *Earth Planet. Sci. Lett.* **213**, 15 (2003).
12. N. J. Beukes, *Sediment. Geol.* **54**, 1 (1987).
13. C. Klein, N. J. Beukes, *Econ. Geol.* **84**, 1733 (1989).
14. N. J. Beukes, C. Klein, A. J. Kaufman, J. M. Hayes, *Econ. Geol.* **85**, 663 (1990).
15. B. Krapež, M. E. Barley, A. L. Pickard, *Sedimentology* **50**, 979 (2003).
16. J. J. Brocks, R. Buick, G. A. Logan, R. E. Summons, *Geochim. Cosmochim. Acta* **67**, 4289 (2003).
17. A. Bekker *et al.*, *Nature* **427**, 117 (2004).
18. All bulk samples were analyzed by the sulfur monoxide method in triplicate, and the reported values are averages of these measurements. Uncertainties are better than 0.3‰ for both $\delta^{34}S$ and $\Delta^{33}S$ values, which is comparable with uncertainties based on multiple standard measurements during each analytical session. For SF_6 analyses, uncertainties are 0.14, 0.008, and 0.20‰ for $\delta^{34}S$, $\Delta^{33}S$, and $\Delta^{36}S$, respectively.
19. Monte Carlo resampling of data suggests that the two intervals carry a unique isotopic mean. In the lower half, we calculated means of $\delta^{34}S = 3.04$ (±0.50) and $\Delta^{33}S = 1.98$ (±0.44). In the upper half, including the organic and pyrite-rich horizon, the data indicate means of $\delta^{34}S = -1.41$ (±0.34) and $\Delta^{33}S = 1.10$ (±0.29). Considered alone, data from the pyritic interval between 153 and 135 m indicate means of $\delta^{34}S = -0.80$ (±0.47) and $\Delta^{33}S = -0.54$ (±0.17).
20. Atmospheric photochemistry is presently the only known mechanism that can account for the nonzero $\Delta^{33}S$ data and their relationship to $\Delta^{36}S$ values in the Archean record (*1*–*4*, *17*). The principal source of S in the Archean atmosphere was volcanic (although biogenic sources may have also existed). Gas-phase photochemistry involving sulfur dioxide or sulfur monoxide has been shown in closed-cell photochemical experiments (*2*) to result in NMD sulfate (SO_4^{2-}; with negative, and in some cases positive, $\Delta^{33}S$ values) and elemental S (S_8, with positive $\Delta^{33}S$ values). These reactions are sensitive to the wavelength of available ultraviolet radiation, and this parameter depends on, among other things, atmospheric O_2 concentrations. The transfer pathways of S from the atmosphere to Earth's surface also depend on O_2 concentration. An atmospheric model (*4*) constrains an upper limit of $<10^{-5}$ of present atmospheric levels of O_2 for the transfer of nonzero $\Delta^{33}S$ (and $\Delta^{36}S$) containing SO_4^{2-} and S_8 to Earth's surface; at a higher partial pressure of O_2, the two S reservoirs homogenize in the atmosphere, and the photochemical signal is not preserved.
21. B. S. Kamber, M. J. Whitehouse, *Geobiology* **5**, 5 (2006).
22. K. S. Habicht, M. Gade, B. Thamdrup, P. Berg, D. E. Canfield, *Science* **298**, 2372 (2002).
23. This interpretation is based on the assumption that S metabolisms operating at the Archean/Proterozoic boundary are similar to those of today. At present, we see no other realistic environmental scenario that could account for the unusual S isotope compositions of the upper Mount McRae Shale.
24. D. R. Lovley, E. J. P. Phillips, *Appl. Environ. Microbiol.* **60**, 2394 (1994).
25. D. T. Johnston *et al.*, *Science* **310**, 1477 (2005).
26. B. Fry, J. Cox, H. Gest, J. M. Hayes, *J. Bacteriol.* **165**, 328 (1986).
27. J. Farquhar, B. A. Wing, in *Mineral Deposits and Earth Evolution*, I. McDonald, A. J. Boyce, I. B. Butler, R. J. Herrington, D. A. Polya, Eds. (Geol. Soc. London Spec. Pub., London, 2005), vol. 248, pp. 167–177.
28. A Monte Carlo resampling of the entire Mount McRae data set ($\Delta^{33}S = 1.25 \pm 0.17$), which mirrors that of the entire Archean (*27*), points to a negative $\Delta^{33}S$ reservoir of the Archean S cycle largely lost from the geological record. Evidence from banded iron-formations, volcanic massive sulfide deposits, and other sea-floor environments may ultimately provide tests for a sulfate concentration gradient in the Archean ocean and solve the mystery of the missing negative $\Delta^{33}S$ reservoir. Ultimately, the balance of sources and sinks maintained generally low sulfate concentrations that allowed for spatial isotopic heterogeneities.
29. A. G. Harrison, H. G. Thode, *Trans. Faraday Soc.* **54**, 84 (1958).
30. S. Ono *et al.*, *Geochim. Cosmochim. Acta* **70**, 2238 (2006).
31. J. Farquhar, J. Savarino, T. L. Jackson, M. H. Thiemens, *Nature* **404**, 50 (2000).
32. D. T. Johnston *et al.*, *Geochim. Cosmochim. Acta* **70**, 5723 (2006).
33. H. Ohmoto *et al.*, *Nature* **442**, 908 (2006).
34. J. Farquhar *et al.*, *Geochim. Cosmochim. Acta* **71**, A269 (2007).
35. Mass-dependent recycling has not been used to substantially alter the $\Delta^{36}S/\Delta^{33}S$ relation of Archean samples, but recycling by processes associated with the establishment of an oxidative S cycle in the surface ocean may also account for some of the variation due to the different (~–7) $\Delta^{36}S/\Delta^{33}S$ slopes.
36. A. J. Kaufman, *Precambrian Res.* **79**, 171 (1996).
37. E. S. Cheney, *Precambrian Res.* **79**, 3 (1996).
38. We thank the NASA Astrobiology Institute and the Geological Survey of Western Australia for drilling of the ABDP-9 core; the NSF for scientific funding for the project; J. S. R. Dunlop, L. C. Bonser, M. van Kranendonk, A. Hickman, and the Geological Survey of Western Australia for assisting with core recovery; B. Runnegar and R. Grymes for launching the Astrobiology Drilling Program; A. H. Knoll for long-term support of the project; J. Kasting, B. Simonson, and anonymous reviewers for their comments and suggestions; and the Gas Source Mass Spectrometry research staff at the University of Maryland, including N. Collins, K. Yokoyama, B. Williams, and A. Shrestha for their analytical efforts. Samples from the AD-5 core were provided to N. Beukes, C. Klein, and A.J.K. by Griqualand Exploration and Finance Company in South Africa.

Supporting Online Material

www.sciencemag.org/cgi/content/full/317/5846/1900/DC1
SOM Text
Figs. S1 to S4
Tables S1 and S2
References

11 December 2006; accepted 16 August 2007
10.1126/science.1138700

A Whiff of Oxygen Before the Great Oxidation Event?

Ariel D. Anbar,[1,2]* Yun Duan,[1] Timothy W. Lyons,[3] Gail L. Arnold,[1] Brian Kendall,[4] Robert A. Creaser,[4] Alan J. Kaufman,[5] Gwyneth W. Gordon,[1] Clinton Scott,[3] Jessica Garvin,[6] Roger Buick[6]

High-resolution chemostratigraphy reveals an episode of enrichment of the redox-sensitive transition metals molybdenum and rhenium in the late Archean Mount McRae Shale in Western Australia. Correlations with organic carbon indicate that these metals were derived from contemporaneous seawater. Rhenium/osmium geochronology demonstrates that the enrichment is a primary sedimentary feature dating to 2501 ± 8 million years ago (Ma). Molybdenum and rhenium were probably supplied to Archean oceans by oxidative weathering of crustal sulfide minerals. These findings point to the presence of small amounts of O_2 in the environment more than 50 million years before the start of the Great Oxidation Event.

Many lines of evidence point to a rapid rise in the partial pressure of atmospheric O_2 (P_{O_2}) from $<10^{-5}$ times the present atmospheric level (PAL) between 2.45 and 2.22 billion years ago (Ga) (*1*, *2*), a transition often referred to as the Great Oxidation Event (GOE). The GOE could have been an immediate consequence of the evolution of oxygenic photosynthesis (*3*). Alternatively, O_2 biogenesis may be ancient (*4*). If so, the GOE was a consequence of an abiotic shift in the balance of oxidants and reductants at Earth's surface (*5*–*8*). This debate can be addressed by looking for evidence of localized or short-lived concentrations of O_2 before 2.45 Ga.

The abundances of some transition elements in sedimentary rocks are sensitive to the availability of O_2 (*9*). In particular, in the modern oxygenated environment, molybdenum (Mo) exists in rivers and oceans primarily as the unreactive molybdate ion (MoO_4^{2-}). Oxidative weathering of Mo-bearing sulfide minerals in crustal rocks leads to the accumulation of Mo in the oceans, where it is the most abundant transition element (at a concentration of ~105 nM) (*10*, *11*). The abundance of Mo in the oceans is reflected in

[1]School of Earth and Space Exploration, Arizona State University, Tempe, AZ 85287, USA. [2]Department of Chemistry and Biochemistry, Arizona State University, Tempe, AZ 85287, USA. [3]Department of Earth Sciences, University of California, Riverside, CA 92521, USA. [4]Department of Earth and Atmospheric Sciences, University of Alberta, Edmonton, Alberta, Canada T6G 2E3. [5]Department of Geology, University of Maryland, College Park, MD 20742, USA. [6]Department of Earth and Space Sciences, University of Washington, Seattle, WA 98195, USA.

*To whom correspondence should be addressed. E-mail: anbar@asu.edu

pyritic marine sediments deposited under oxygen-deficient conditions, where Mo is removed from solution in association with organic carbon (*12*, *13*), probably after reacting with H_2S to form oxythiomolybdates ($MoO_{4-x}S_x^{2-}$) (*14*). In such sediments deposited today and through much of the Phanerozoic, Mo contents are typically >100 ppm versus ~1 ppm in average crust (*10*, *12*, *13*, *15*, *16*).

By comparison, on an anoxic Earth, Mo would be largely retained in unoxidized crustal sulfide minerals during weathering. Therefore, Mo concentrations in the oceans would be low, and organic-rich sediments would show little authigenic Mo enrichment as compared to modern equivalents. Similar logic applies to sulfur (S). In fact, studies of Mo and S concentrations and stable isotopes in black shales reveal systematic shifts in ocean budgets from the Archean through the Phanerozoic that are broadly consistent with the GOE and with another rise in P_{O_2} later in the Proterozoic (*2*, *17*–*19*) (table S1). Rhenium (Re) and uranium (U) are also promising indicators because their aqueous geochemistry is similar to that of Mo.

Here we report Mo, Re, U, and S measurements, as well as other geochemical data obtained at high stratigraphic resolution in the Mount McRae Shale, deposited ~2.5 Ga in the Hamersley Basin, Western Australia (*20*, *21*). Approximately 100 samples were analyzed from a freshly recovered continuous drill core obtained for this study (*22*) (Fig. 1, fig. S1, and table S2). These samples were also analyzed for S isotope variations as part of a companion study (*23*).

The core intersected two intervals containing pervasive pyritic carbonaceous shale, which we refer to as S1 (from 125.5 to 153.3 m) and S2 (from 173.0 to 189.65 m). Shales in both intervals contain several weight % (wt %) S and typically >3% total organic carbon (TOC), which is consistent with anoxic (and potentially sulfidic) bottom waters and the presence of H_2S in pore waters during these depositional intervals.

The most prominent feature of the data is the excursion in Mo content within S1 (Fig. 1). Mo concentrations below this layer are typically <5 parts per million (ppm), which is near the crustal value and is typical of Archean carbonaceous shales. Concentrations increase gradually up the section from the base of S1 to a peak value of ~40 ppm at 143 m and then decrease to <10 ppm by ~125 m. These variations and the Mo peak at ~143 m are more pronounced when plotted as aluminum (Al)–normalized enrichment factors (*24*). Viewed this way, Mo content increases up the section by ~50 times before falling sharply over an interval of ~2 m. The Mo enrichment correlates with enrichments in TOC and Re and broadly coincides with variations in carbonate and S contents. However, U contents vary little through the section.

The coherent behavior of Mo, Re, and U makes it possible to use Re/Os geochronometry to verify that metal abundances were unaffected by remobilization. Postdepositional addition or loss of Re (or Os) would result in significant isochron scatter. We find that samples taken from 128 to 149 m define an isochron with mean square weighted deviation = 1.1 (*22*) (Fig. 2 and table S3) and an age of 2501.1 ± 8.2 million years, which is consistent with previous ages for the Mount McRae shale (*20*, *21*). The element enrichments are therefore primary sedimentary features (as is the lack of associated U variation) deposited at the boundary of the Archean and Proterozoic eons, at least 50 million years before the beginning of the GOE.

The Mo excursion cannot be explained by variable carbonate dilution, as documented by extreme enrichment factors (Fig. 1). Instead, the correlations of Mo with TOC are strong evidence of authigenic enrichment (Fig. 3). Such trends are common in sediments from modern anoxic

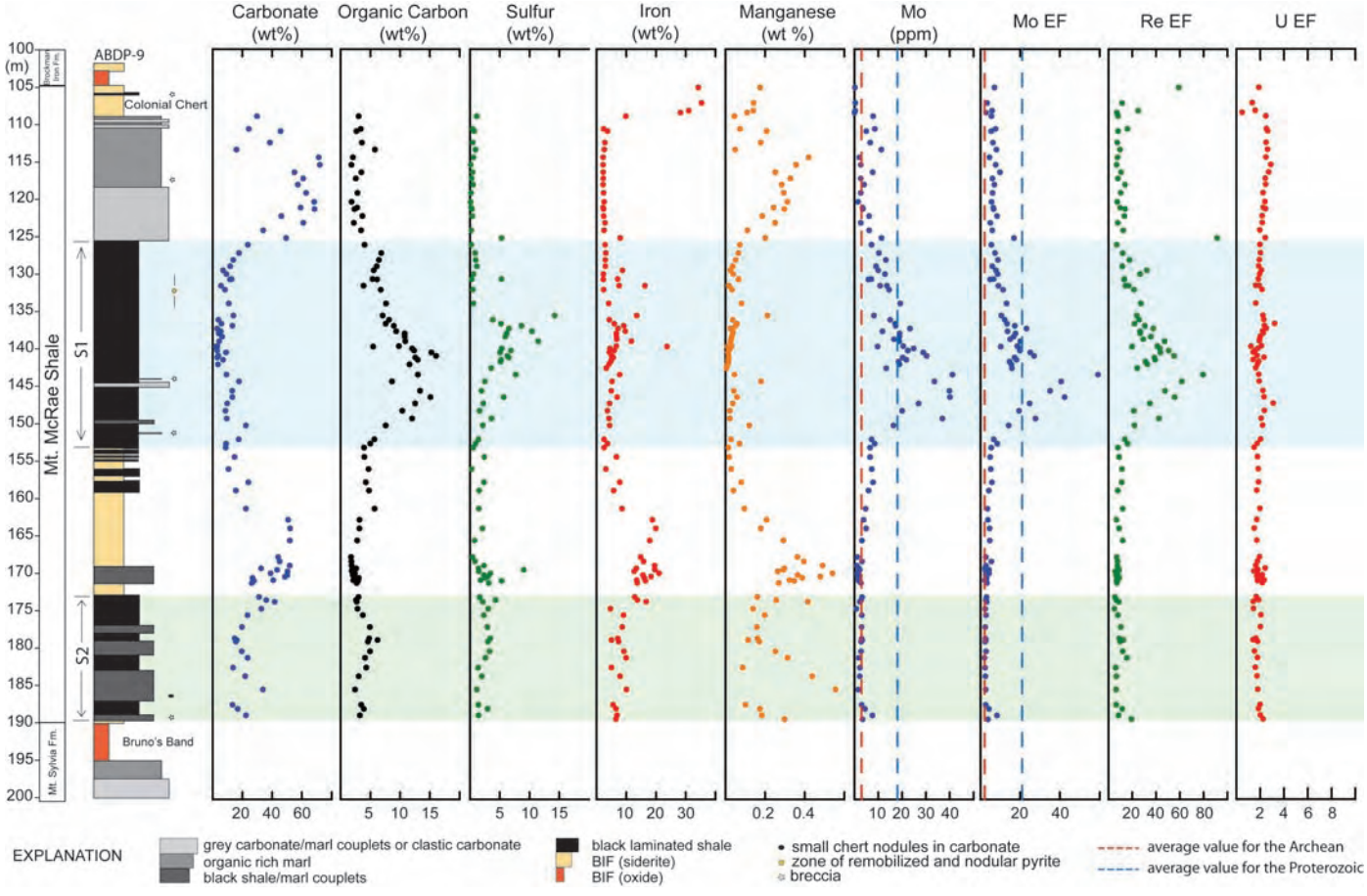

Fig. 1. Stratigraphy and geochemistry of the Mount McRae Shale, including percent of carbonate, TOC, S, Fe, Mn, Mo, Re, and U and EFs (*24*) for Mo, Re, and U (*23*). The intervals S1 and S2 span 125.5 to 153.3 m and 173.0 to 189.7 m, respectively. For comparison, dashed lines denote mean Mo concentrations and EFs in Archean and Proterozoic pyritic black shales, as indicated in the legend at bottom (*18*, *22*) (tables S1 and S2).

basins where the concentration of H_2S exceeds ~10 μM. In such sediments, Mo/TOC scales with Mo concentrations in deep waters (*12*). We recognize two trends within S1, corresponding to the zone of increasing Mo enrichment (~143 to 153 m) and the overlying zone in which Mo falls but remains elevated above average crustal values (~125 to 143 m). Mo/TOC slopes in these zones are ~3.4 ± 0.5 (±1σ) ppm Mo/wt % TOC and ~1.8 ± 0.2 (±1σ) ppm Mo/wt % TOC, respectively (*25*). By comparison, Mo/TOC is 4.5 to 25 ppm Mo/wt % TOC in pyritic sediments from modern anoxic basins (*12*) and averages ~26 ppm Mo/wt % TOC in Phanerozoic pyritic black shales (*18*) (table S1). Hence, small but substantial concentrations of dissolved Mo were present during S1 deposition. Similar reasoning can be applied to Re (fig. S2A).

These observations are not easily explained by hydrothermal inputs to the oceans. Enhanced hydrothermal input should result, first and foremost, in enrichments of iron (Fe) and manganese (Mn), yet the S1 unit is depleted in these elements relative to S2. In any event, high-temperature mid-ocean ridge–type systems should be sinks, not sources, for Mo and Re because of the low solubilities of Mo and Re sulfides. A small amount of Mo enters seawater today as result of low-temperature hydrothermal seafloor weathering (*13*), but this Mo is probably derived from modern Mo-rich seafloor sediments.

Instead, these observations can be straightforwardly interpreted as evidence of oxidative weathering during S1 deposition. We hypothesize that O_2 in the shallow oceans and possibly in the atmosphere enhanced the rate of dissolution of submarine and subaerial sulfide minerals, such as molybdenite (MoS_2), that are important for the budgets of Mo and Re in igneous and metamorphic crustal rocks. Mo and Re released in this way would ultimately have produced authigenic enrichments in ocean sediments.

Sulfide minerals weather rapidly in the presence of O_2, so P_{O_2} need not have been high. For example, even if P_{O_2} is only ~10^{-5} PAL, a pyrite crystal of 100 μm^3 volume will dissolve completely in <~20,000 years (*26*, *27*). This is a short time compared to the likely duration of S1 (*28*). Consistent with such low P_{O_2}, Mo/TOC values in S1 do not exceed those of sediments accumulating in the modern Black Sea, which implies that the concentration of Mo in contemporaneous seawater was of similar magnitude as that in the deep waters of the Black Sea, or <1% that of fully oxygenated modern oceans.

The same process could have contributed to the excursion in S content and $\delta^{34}S$ in S1 (*23*). The long-term $\delta^{34}S$ record of sedimentary sulfides exhibits a negative shift between 2.4 and 2.3 Ga that is thought to indicate an increase in ocean sulfate concentrations. This increase is ascribed to an increased rate of oxidative weathering of pyrites in crustal rocks during and after the GOE (*2*). The negative shift in sedimentary $\delta^{34}S$ beginning at ~153 m in the Mount McRae Shale may record the effects of less extreme oxygenation at 2.5 Ga.

Our hypothesis of mild oxygenation is supported by the absence of U enrichment coincident with Mo and Re enrichments (Fig. 1) and the lack of correlation between U and TOC in S1 (fig. S2B), observations indicating that dissolved U concentrations were very low. U in the crust is primarily hosted by feldspars, zircon, apatite, and sphene, but not sulfides. Therefore the rate of release of U from rocks is only weakly affected by oxygenation, unlike that of Mo and Re; experimental studies suggest that the rate of pyrite oxidation exceeds that of feldspar minerals when $P_{O_2} > 10^{-6}$ PAL (*29*, *30*). U may also be less mobile than Mo and Re when O_2 is low (*31*). Hence, enhancements of Mo and Re influx without U enhancement are expected in the presence of small amounts of O_2.

Our interpretation is also consistent with the extremely nonradiogenic initial $^{187}Os/^{188}Os$ in the Mount McRae Shale (Fig. 2). Such low values, also seen in shales ~200 million years younger (*32*), indicate that the ocean Os budget was dominated by hydrothermal sources rather than by radiogenic Os derived from the weathering of high-Re/Os crustal rocks. As with U, oxidative weathering of sulfide minerals in igneous or metamorphic rocks might have had little effect on the balance between hydrothermal and crustal sources of Os to the oceans, because the Os content of crustal sulfide minerals, particularly molybdenite, can be low.

The low levels of O_2 that can account for our data are similar to the upper limit of 10^{-5} PAL for typical Archean P_{O_2} derived from the observation of nonzero $\Delta^{33}S$ in Archean sediments (*33*, *34*), possibly explaining the juxtaposition of Mo and Re enrichments with the small nonzero $\Delta^{33}S$ signals seen throughout S1 (*23*). Alternatively, P_{O_2} above this threshold could have been present ephemerally within geographically restricted areas such as biologically productive regions of the oceans.

In contrast to the observations in S1, Mo concentrations and enrichment factors are very low below ~153 m, including in the organic carbon–rich and pyritic S2, where Mo is essentially invariant with TOC [Mo/TOC = 0.15 ±

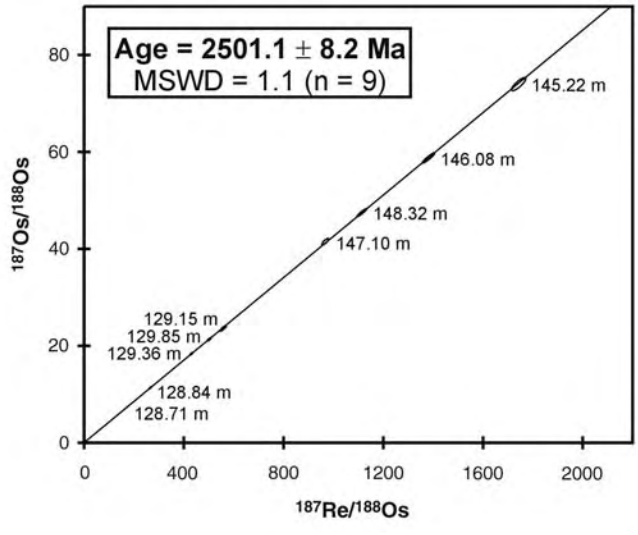

Fig. 2. Re/Os isochron from the Mount McRae Shale, based on data from two subintervals within S1 (128.71 to 129.85 m and 145.22 to 148.32 m). MSWD, mean square weighted deviation. The Re/Os age, 2501.1 ± 8.2 Ma (initial $^{187}Os/^{188}Os$ = 0.04 ± 0.06), falls between prior ages of 2479 ± 3 Ma for the overlying Dales Gorge Member of the Brockman Iron Formation (*20*) and 2561 ± 8 Ma for the underlying Bee Gorge Member of the Wittenoom Formation (*21*). Details are discussed in (*22*).

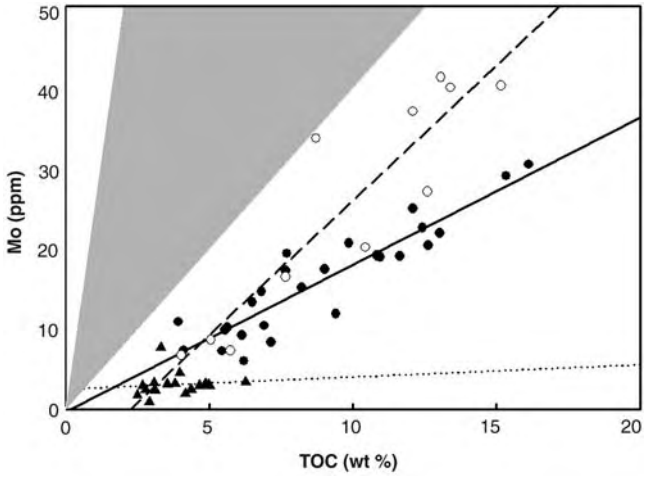

Fig. 3. Relationship between Mo and TOC in organic carbon-rich pyritic intervals in the Mount McRae Shale. Circles are from interval S1 (125.5 to 153.3 m). The metal-enriched zone of S1 below 143 m (open circles) is differentiated from the upper zone (solid circles). Triangles are from interval S2 (173.0 to 189.7 m). For comparison, the shaded region indicates the range of Mo/TOC slopes (forced through the origin) observed in modern sulfide-rich anoxic basins.

0.35 (±1σ) ppm Mo/wt % TOC] (Fig. 3). Weak correlations appear between Mo and Al in S2, suggesting that at these depths the Mo budget was influenced by detrital components; such correlations are absent from S1. These observations point to much less authigenic Mo enrichment in S2 than in S1.

The difference in Mo enrichment suggests that the Mo inventory in overlying waters was much larger during S1 deposition than during S2 deposition, as would follow from an increase in environmental oxygenation up the section beginning at ~153 m. This interpretation is complicated by the fact that the Mo concentration differences between the units were also affected by differences in local depositional conditions that increased the efficiency with which Mo was transferred from water to sediments during S1 time (*35*). However, a difference in the dissolved Mo inventory and in ocean oxygenation provides a compelling explanation for the sharp difference in Mo/TOC between the units (*36*).

Other data from the core also point to greater surface ocean oxygenation above ~153 m, including changes in $\delta^{34}S$-$\Delta^{33}S$ systematics that may record the onset of an oxidative sulfur cycle (*23*). A redox shift can also explain differences in Fe and Mn concentrations above and below ~160 m (Fig. 1). Below this depth, most of the Fe is present as siderite ($FeCO_3$), and both elements are much lower in S1 than in S2. Fe and Mn would have been easily mobilized during anoxic weathering, enriched in anoxic S-poor Archean oceans and hence available for incorporation into sediments. Oxygenation of surface environments would have reduced the availability of both elements. At the same time, Re concentrations are slightly elevated above crustal average values throughout the core, and there is a positive correlation of Re with TOC in S2 as well as S1 (fig. S2B). Re can be more mobile than Mo during oxidative sulfide weathering (*37*), so this persistent Re enrichment suggests that some small degree of oxidative weathering occurred throughout.

The decrease in Mo content and Mo/TOC above 143 m may record a drop in the dissolved Mo inventory after its initial rise, even though the surface environment apparently remained persistently, if mildly, oxygenated (*23*). Re and S also decrease. Diagenetic complications notwithstanding (*23*), it is tempting to speculate that these decreases mirror a drop in atmosphere or ocean redox potential (*38*), as a result of biological or nonbiological feedbacks (*39*). However, declining trace metal abundances could simply reflect the exhaustion of exposed crustal sulfide sources, or areal expansion of sulfidic basins in the oceans in response to rising sulfate reduction, drawing down seawater Mo, Re, and S inventories.

The onset of oxidative weathering at 2.5 Ga was probably widespread. A recent examination of contemporaneous sediments from the Ghaap Group in South Africa found that authigenic Mo and Re increased between 2.64 and 2.5 Ga (*40*), although that study did not have the stratigraphic resolution to capture the scale of variations reported here. Changes in S isotope systematics like those in the Mount McRae Shale also appear in time-correlative units from South Africa (*23*). Theoretical models show that a shift toward more oxidizing conditions can occur before the rise of an oxygenated atmosphere (*5*). Hence, the whiff of oxygen in the Mount McRae Shale may presage the global and irreversible transition to an oxygenated world.

References and Notes

1. A. Bekker *et al.*, *Nature* **427**, 117 (2004).
2. D. E. Canfield, *Annu. Rev. Earth Planet. Sci.* **33**, 1 (2005).
3. R. E. Kopp, J. L. Kirschvink, I. A. Hilburn, C. Z. Nash, *Proc. Natl. Acad. Sci. U.S.A.* **102**, 11131 (2005).
4. J. J. Brocks, G. A. Logan, R. Buick, R. E. Summons, *Science* **285**, 1033 (1999).
5. M. W. Claire, D. C. Catling, K. J. Zahnle, *Geobiology* **4**, 239 (2006).
6. C. Goldblatt, T. M. Lenton, A. J. Watson, *Nature* **443**, 683 (2006).
7. L. R. Kump, M. E. Barley, *Nature* **448**, 1033 (2007).
8. H. D. Holland, *Geochim. Cosmochim. Acta* **66**, 3811 (2002).
9. H. D. Holland, *The Chemical Evolution of the Atmosphere and Oceans* (Princeton Univ. Press, Princeton, NJ, 1984).
10. K. K. Bertine, K. K. Turekian, *Geochim. Cosmochim. Acta* **37**, 1415 (1973).
11. R. W. Collier, *Limnol. Oceanogr.* **30**, 1351 (1985).
12. T. J. Algeo, T. W. Lyons, *Paleoceanography* **21**, PA1016 (2006).
13. J. McManus *et al.*, *Geochim. Cosmochim. Acta* **70**, 4643 (2006).
14. G. R. Helz *et al.*, *Geochim. Cosmochim. Acta* **60**, 3631 (1996).
15. J. L. Morford, S. Emerson, *Geochim. Cosmochim. Acta* **63**, 1735 (1999).
16. S. R. Taylor, S. M. McLennan, *Rev. Geophys.* **33**, 241 (1995).
17. G. L. Arnold, A. D. Anbar, J. Barling, T. W. Lyons, *Science* **304**, 87 (2004).
18. C. T. Scott, T. W. Lyons, A. D. Anbar, *Geochim. Cosmochim. Acta* **68**, A787 (2004).
19. C. Siebert, J. D. Kramers, T. Meisel, P. Morel, T. F. Nagler, *Geochim. Cosmochim. Acta* **69**, 1787 (2005).
20. D. R. Nelson, A. F. Trendall, W. Altermann, *Precambrian Res.* **97**, 165 (1999).
21. A. F. Trendall, D. R. Nelson, J. R. De Laeter, S. W. Hassler, *Aust. J. Earth Sci.* **45**, 137 (1998).
22. Materials, methods, and supplemental data are available as supporting material on *Science* Online.
23. A. J. Kaufman *et al.*, *Science* **317**, 1900 (2007).
24. Enrichment factors (EFs) = $(metal/Al)_{sample}/(metal/Al)_{reference}$. Here, the reference is average crust (*16*). This normalization compensates for variable dilution by carbonate sedimentation and facilitates visualization of authigenic enrichment.
25. Mo/TOC slopes are probably now steeper than they were at the time of deposition, because organic carbon is preferentially lost during catagenesis.
26. M. A. Williamson, J. D. Rimstidt, *Geochim. Cosmochim. Acta* **58**, 5443 (1994).
27. This dissolution time assumes that a detrital pyrite crystal is exposed on all sides to water in equilibrium with O_2 at pH > 5 and temperature < 70°C. The weathering rate is only slightly sensitive to temperature but roughly doubles if pH increases to a typical marine value of ~8.3. These rates are lower limits because they neglect the rate-enhancing effects of crystal defects and microbial activity.
28. The duration of S1 is difficult to estimate but is <16 million years based on the uncertainty in the Re/Os isochron. Assuming a typical average shale accumulation rate of ~2.5 m/million years, the duration is ~11 million years. These estimates are consistent with accumulation rates determined from prior geochronology of sampled units (*20*, *21*).
29. A. E. Blum, L. L. Stillings, *Rev. Mineral.* **31**, 291 (1995).
30. This rate assumes pH = 5 and P_{CO_2} ~ 20 PAL. Higher P_{O_2} would be required if CO_2 were higher, because feldspar weathering rate is a strong function of pH.
31. Soluble U^{6+} can be converted to insoluble U^{4+} under conditions similar to those that favor the reduction of Fe^{3+} to Fe^{2+}; that is, environments that are anoxic or "suboxic" (*13*). By comparison, efficient immobilization of Mo appears to occur in settings that are reducing enough that H_2S appears in sediment porewaters.
32. J. L. Hannah, A. Bekker, H. J. Stein, R. J. Markey, H. D. Holland, *Earth Planet. Sci. Lett.* **225**, 43 (2004).
33. J. Farquhar, B. A. Wing, *Earth Planet. Sci. Lett.* **213**, 1 (2003).
34. A. A. Pavlov, J. F. Kasting, *Astrobiology* **2**, 27 (2002).
35. For example, the sequestration of Mo into reducing sediments is affected by the flux of organic carbon and water-column H_2S concentrations, so delivery of Mo to sediments can be affected by changes in primary production, sulfate availability, or the vigor of bacterial sulfate reduction.
36. We interpret this stratigraphic shift as indicating a change in environmental oxygenation with time. It is alternatively possible that the shift records sediments accumulating at different water depths in a redox-stratified water column. In either case, the Mo and Re enrichments are evidence of oxidative weathering ~2.5 Ga.
37. D. E. Morachevskii, A. A. Nechaeva, *Geochemistry* **6**, 649 (1960).
38. Consistent with this notion, the rise in Mn content in carbonates above ~125 m without the associated Fe observed deeper in the core indicates segregation of these metals in waters that were only mildly oxygenated. Fe^{2+} and Mn^{2+} are immobile when oxidized to Fe^{3+} and Mn^{4+}, respectively, because of the formation of insoluble oxyhydroxides. However, Fe^{2+} is oxidized at a lower Eh than Mn^{2+}. Segregation is also facilitated by the slower oxidation and hydrolysis kinetics of Mn^{2+} versus Fe^{2+}.
39. For example, biologically, rising O_2 could inhibit N_2 fixation or limit the availability of bioessential Fe, thereby reducing productivity and the rate of O_2 production. Nonbiologically oxidative erosion of a methane greenhouse would lead to lower surface temperatures, hence higher solubility of O_2 in surface oceans, lowering P_{O_2}.
40. M. Wille *et al.*, *Geochim. Cosmochim. Acta* **71**, 2417 (2007).

41. The authors thank A. H. Knoll for inspiration and encouragement; B. Runnegar and R. Grymes for launching the Astrobiology Drilling Program; B. Blumberg for supporting the Mission to Early Earth Focus Group of the NASA Astrobiology Institute; and J. Farquhar, R. Raiswell, D. Johnston, A. Bekker, T. Algeo, J. Kasting, and J. Hannah for helpful discussions. Two anonymous reviewers helped improve the manuscript. J. S. R. Dunlop, L. C. Bonser, M. van Kranendonk, A. Hickman, and the Geological Survey of Western Australia assisted with core recovery. Funding was provided by the NASA Astrobiology Institute and the NSF Geobiology and Low Temperature Geochemistry program.

Supporting Online Material

www.sciencemag.org/cgi/content/full/317/5846/1903/DC1
Materials and Methods
Figs. S1 and S2
Tables S1 to S3

24 January 2007; accepted 16 August 2007
10.1126/science.1140325

Supporting Online Material for

A Whiff of Oxygen Before the Great Oxidation Event?

A. D. Anbar,* Y. Duan, T. W. Lyons, G. L. Arnold, B. Kendall, R. A. Creaser, A. J. Kaufman, G. W. Gordon, C. Scott, J. Garvin, R. Buick

*To whom correspondence should be addressed. E-mail: anbar@asu.edu

Published 28 September 2007, *Science* **317**, 1903 (2007)
DOI: 10.1126/science.1140325

This PDF file includes:

Materials and Methods
Figs. S1 and S2
Tables S1 to S3

Supporting Online Materials
for
A Whiff of Oxygen before the Great Oxidation Event?

The Hamersley Core

The Hamersley core was recovered during the summer of 2004 as part of the Deep Time Drilling Project (DTDP) of the Astrobiology Drilling Program (ADP) of the NASA Astrobiology Institute (NAI). This project also involved the Geological Survey of Western Australia, Randolph Resources, Hamersley Iron, SIPA Resources International, and the University of Western Australia. This was one of ten cores recovered by the ADP in 2003 – 2004; seven others were collected as part of the Archean Biosphere Drilling Project (ABDP) (*1*), and two others were collected in collaboration between the DTDP and the ABDP. Therefore, this core is sometimes referred to as "ABDP-9". The motivation for recovery of this particular core was to obtain drill core free of modern contamination and weathering effects for biogeochemical analysis to characterize the nature of life and its environment in the late Archean, shortly before the rise of atmospheric oxygen.

Approximately 1000 m of continuous drill core spanning banded iron formation, kerogenous shales, basinal carbonates, shallower cherts and clastics, and meteorite impact horizons were recovered. The drill site was located at 21°59'29.5"S, 117°25'13.6"E, hole azimuth 186°, dip 89°, on the Pilbara craton of Western Australia (Figure S1). One half of the core is archived at the Geological Survey of Western Australia's (GSWA) Perth Core Library. The other (working) half of the core is presently stored at the School of Earth and Space Exploration at Arizona State University. For more information about the DTDP or how to request samples, please see http://nai.nasa.gov/ADP/DTDP2004.cfm.

Lithostratigraphy and Sampling

The core intersects laminated and well preserved sediments accumulated in a marine environment below wave base. These sediments have experienced only mild regional metamorphism (prehnite-pumpellyite facies to <300°C) and minimal deformation (gentle folding dips <5°). It is underlain by Mt. Sylvia Formation and capped by the Dales Gorge Member of the Brockman Iron Formation. The uppermost part is characterized by inter-bedded carbonates and grey/black shale with pyrite rarely to sparsely seen, gradually transiting into black shale with increasing pyrite content down section. Pyrite nodules occur massively from 131 m - 134 m followed by a 15 m thick section of black shale with frequent pyrite laminae and abundant pyrite nodules. Following this section, pyrite contents drops downcore as the lithology transitions to siderite banded iron formation (BIF). Continuing below 173 m depth, pyritic back shale becomes dominant again, with carbonate/marl interbeds, until the base of the Mt. McRae Shale. The core was sampled at 0.2 m ~ 2 m intervals for high-resolution analyses. For the purpose of this study sampling specifically avoided pyrite nodules. Laminae were avoided wherever possible. Where pyrite laminae were not avoidable (i.e., ~134 to 143 m) samples are labeled with a "pyl" suffix (Table S2).

Metal Concentration Analyses

Data are presented in Table S2. For each sample a billet was cut (3 cm x 5 cm x 1 cm) from the drill core using a water-cooled diamond blade tile saw. The billets were then broken into < 5 mm chips, without metal contact and ground to < 100 mesh in silicon nitride ball mill vials. For major and trace element analyses powder splits were completely dissolved using a standard HNO_3-HCl-HF silicate digestion method. Trace HF was added to each solution to ensure Mo remained stable in solution. All dissolution and dilution was carried out in Class-10 workspaces within a trace metal cleanlab. Samples were analyzed on a Thermo Scientific X Series Q-ICP-MS (quadrupole inductively coupled plasma mass spectrometer) at the W.M. Keck Foundation Laboratory for Environmental Biogeochemistry at Arizona State University. Major elements (including Al, Fe, and Mn) and trace elements (including Mo, U and Re) were measured in separate analytical sessions against multiple element calibration standards. Internal standards Ge, In, Y and Bi, introduced into the instrument in parallel with all samples and standards, were used to correct for signal drift. Signal intensities for each analyte element were at least 3 times that of the blank and were bracketed by the lowest and the highest standard. Analyte concentration reproducibilites are better than 5 % except for low Re samples (when Re concentrations are ~1.5 ppb, the reproducibility drops to ~8 %.). USGS geochemical reference materials SDO-1 and SCO-1, an organic rich and average shale, respectively, were measured alongside samples to assure measurement accuracy. Analyte concentrations produced for the reference materials agree within error of the published values.

Re/Os Isochron

Data are presented in Table S3. For Re/Os analysis, sample billets were cut at ASU as previously described and subsequently processed at the University of Alberta. Between 15 and 40 g of drillcore material was ground to remove cutting and drilling marks, broken into small chips without metal contact, and powdered in an automated agate mill. Re-Os isotope analyses were carried out at the Radiogenic Isotope Facility of the Department of Earth and Atmospheric Sciences, University of Alberta, using chemical separation and mass spectrometry methods outlined in Creaser et al. (*2*), Selby and Creaser (*3*) and Kendall *et al.* (*4*), including the Cr^{VI}-H_2SO_4 digestion protocol for organic-rich sedimentary rocks. This method minimizes release of detrital Re and Os from the silicate matrix in these rocks by selectively dissolving organic matter that is host to predominantly hydrogenous Re and Os (*3, 4*). Rhenium and Os are loaded onto Ni and Pt filaments, respectively, and analyzed by isotope dilution – negative thermal ionization mass spectrometry (ID-NTIMS). Regression of Re and Os isotope data was performed with the program Isoplot V.3.0 (*5*) using a ^{187}Re decay constant of 1.666 x 10^{-11} $year^{-1}$ (*6-8*), 2σ uncertainties for $^{187}Re/^{188}Os$ and $^{187}Os/^{188}Os$ isotope ratios as determined by numerical error propagation, and the error correlation function (rho) (*4*).

Rhenium (11-39 ppb) and Os (467-1148 ppt) are strongly enriched in these shales relative to average present-day upper continental crust (~ 2 ppb Re and 30-50 ppt Os; *9-13*). In addition, Re shows a pronounced enrichment in shales from the 145.22-148.32 m interval (22-39 ppb Re) relative to the 128.71-129.85 m interval (11-21 ppb). Isotope ratios for $^{187}Re/^{188}Os$ and $^{187}Os/^{188}Os$ range from 173 to 558 and from 7.4 to 74.0, respectively. Regression of the Re-Os

isotope data yields Model 1 dates of 2495 ± 18 Ma (2σ, n = 5, MSWD = 0.95, initial $^{187}Os/^{188}Os = 0.06 \pm 0.09$) and 2464 ± 41 Ma (2σ, n = 4, MSWD = 0.48, initial $^{187}Os/^{188}Os = 0.86 \pm 0.86$) for the 128.71-129.85 m and 145.22-148.32 m intervals, respectively. Combining the two data sets yields a Model 1 Re-Os date of 2501.1 ± 8.2 Ma (MSWD = 1.1, initial $^{187}Os/^{188}Os = 0.04 \pm 0.06$).

The initial $^{187}Os/^{188}Os$ isotope composition derived from the regression records the Os isotope composition of the contemporaneous seawater at the time of sediment deposition (*e.g.*, *14*). Because the residence time of Os in present-day seawater is geologically short (~ 10^4-10^5 years; *15, 16*), it is usually necessary to restrict stratigraphic sampling intervals to ~ 1 m or less to avoid initial Os isotope heterogeneity (e.g., *2-4, 7, 17*). The sedimentation rate of the McRae Shale is not known, but during the span of geologic time covered by the ~ 20 m of stratigraphy sampled here, the Os isotope composition of ~ 2.5 Ga seawater probably changed. Accordingly, the Re-Os regression for the 128.71-129.85 m interval provides the most accurate and precise estimate of the $^{187}Os/^{188}Os$ isotope composition of 2.5 Ga seawater (0.06 ± 0.09). This value overlaps the present-day Os isotope composition of chondrites and estimated values for the convecting and primitive upper mantle (~ 0.13; *18-20*) and the Os isotope composition of chondrites at ca. 2.5 Ga (~ 0.11). These data indicate that the ocean Os budget was dominated by hydrothermal fluids and associated low-and high-T hydrothermal alteration of oceanic crust (*21, 22*), weathering of predominantly mafic rocks (*23*), and/or dissolution of cosmic dust.

Total Organic Carbon Analyses

Total organic carbon (TOC) was analyzed at the University of Washington using splits from the same powders analyzed for metals. In preparation for analyses, crushed rock powders were treated with HCl to remove any carbonate present. Specifically, ~10 ml of 36.5 – 38.0 % HCl were added to ~0.3-0.5 g of sample and placed in a 65°C water bath overnight. The acidified samples were rinsed twice with Milli-Q water and dried in a 65°C oven. Samples were weighed before and after acidification to determine the fraction of carbonate. Tin capsules (5x9 mm) containing 0.1 – 0.2 mg of acidified sample were then prepared and analyzed via a Costech ECS 4010 Elemental Analyzer, coupled to a Thermo Scientific MAT 253. Samples were measured in triplicate to ensure reproducibility and those that did not meet a specific criterion ($range_{TOC} \leq 0.5$ ‰; $standard\ deviation_{TOC} \leq 0.4$ ‰) were re-analyzed until they did. An acetanilide reference material with known carbon content (71.09%) was analyzed at the beginning of each run and then after every two sets of triplicates. The TOC of the samples can be determined since the sum of the areas under the three CO_2 peaks (masses 44, 45, and 46) as reported by the mass spectrometer is proportional to the weight of carbon in the sample being analyzed. Because the weight % C of the standard is known, a relationship between the sum of the areas and the weight of carbon needed to produce this sum can be determined. Applying the above relationship to the sum of the areas under the sample peaks gives the weight % C of the samples analyzed. Assuming that all carbonate carbon in the samples is lost during acidification, the calculated weight % C actually represents the weight % organic C of the acidified samples. The TOC values of the bulk samples are then determined by multiplying this value by the fraction of sample remaining after acidification.

Table S1. Average Mo data for Archean and Proterozoic pyritic black shales.

	Average Maximum Mo (ppm)	Average Minimum Mo (ppm)	Average Mo (ppm)	Average Mo/Al (ppm/wt%)	Average Mo/TOC (ppm/wt%)
Archean *	4	1	3	0.4	1.6
Proterozoic **	48	9	18	4	6
Phanerozoic**	270	60	160	27	28

*Yamaguchi (24); **Scott et al. (26)

Table S2. Geochemical data for McRae Shale samples.

	depth (m)		Al wt %	Mn wt %	Fe wt %	Mo ppm	Re ppb	U ppm	Carbonate wt %	TOC wt %	S wt %	Mo/TOC ppm/wt%	Mo/Al ppm/wt%	Re/Al ppb/wt%	U/Al ppm/wt%
ave upper crust*			8.04	0.06	3.5	1.50	1.00**	2.80					0.19	0.12	0.35
													Enrichment Factor	**Enrichment Factor**	**Enrichment Factor**
	105.20		0.3	0.18	34.4	0.4	2.2	0.2					7.3	59.5	1.9
	107.25		0.8	0.14	35.5	0.6	1.2	0.4					3.6	11.7	1.4
	108.27		0.5	0.14	31.1	0.5	1.5	0.3					6.1	25.3	1.6
	108.54		0.3	0.11	28.4	0.2	0.3	0.1					3.1	7.4	0.5
	109.00		7.5	0.05	10.0	8.0	7.9	6.6	30.1	3.1	1.2	2.6	5.7	8.5	2.5
	110.70		5.9	0.08	2.5	8.7	12.1	5.3	24.6	3.5	0.5	2.5	7.8	16.3	2.6
	111.00		4.8	0.21	3.9	5.1	5.1	4.5	46.0	2.7	0.8	1.9	5.7	8.5	2.7
	112.52		5.6	0.18	3.0	6.8	5.5	4.9	38.8	3.7	0.5	1.9	6.5	7.8	2.5
	113.46		7.5	0.05	2.7	11.5	9.4	6.9	16.3	5.8	1.0	2.0	8.2	10.1	2.7
	114.50		2.5	0.42	2.3	2.2	2.5	2.2	71.6	2.2	0.7	1.0	4.8	8.0	2.5
	115.49		1.9	0.36	2.4	2.8	1.7	1.9	72.4	1.9	0.2	1.5	7.9	7.2	2.9
	116.49		4.2	0.25	2.4	7.8	5.7	4.0	55.3	3.6	0.5	2.2	10.1	11.0	2.7
	117.31		2.4	0.33	2.4	2.8	2.5	2.1	61.2	2.6	0.3	1.1	6.3	8.4	2.5
	118.13		3.2	0.29	2.3	4.3	5.7	2.7	57.6		0.6		7.2	14.4	2.5
	119.24		2.4	0.30	2.5	2.8	3.2	1.9	63.1	2.9	0.2	1.0	6.3	10.7	2.3
	120.42		1.6	0.31	2.7	1.7	1.5	1.3	68.6	1.9	0.2	0.9	5.8	7.7	2.4
	121.20		2.9	0.25	2.4	3.6	3.6	2.3	59.5	2.9	0.3	1.2	6.7	10.2	2.3
	121.39		2.9	0.30	2.5	3.7	5.2	2.5	68.8	2.4	0.4	1.5	6.8	14.4	2.5
	122.32		3.9	0.19	2.6	6.3	6.8	3.0	46.5	3.7	0.4	1.7	8.6	13.8	2.2
	123.22		2.9	0.25	3.0	2.8	2.9	2.2	61.3	2.3		1.2	5.2	8.2	2.2
	124.22		5.5	0.11	2.7	6.3	8.7	3.8	34.4	3.5	0.3	1.8	6.2	12.7	2.0
	125.25		3.6	0.20	8.1	11.5	41.1	3.1	49.7		5.4		17.1	91.7	2.5
S1	126.15		6.9	0.07	3.0	7.4	6.2	4.8	24.0	4.1	0.3	1.8	5.7	7.3	2.0
	127.25		7.4	0.07	3.2	10.4	11.3	5.3	18.0	6.9	0.9	1.5	7.6	12.4	2.1
	128.17		7.9	0.05	3.1	13.3	17.8	5.4	14.2	6.5	1.0	2.1	9.0	18.1	2.0
	129.01		8.1	0.04	3.1	9.2	12.0	5.4	12.1	6.1	1.2	1.5	6.1	12.0	1.9
	129.55		6.8	0.03	8.9	10.2	27.6	5.1	7.3	5.6		1.8	8.0	32.6	2.1
	130.06		7.8	0.04	2.5	13.0	26.2	5.4	9.5		0.7		8.9	27.0	2.0
	130.71	-pyl	5.7	0.07	7.3	7.3	9.7	3.7	13.0	5.5	5.4	1.3	6.8	13.7	1.9
	130.76		6.3	0.07	2.4	6.0	10.7	4.2	12.0	6.2	0.4	1.0	5.1	13.6	1.9
	131.60		8.0	0.02	7.8	13.8	17.3	5.4					9.2	17.4	1.9
	131.60		6.3	0.02	16.4	10.9	11.5	3.6	5.9	3.9		2.8	9.2	14.6	1.7
	132.13		6.8	0.04	2.5	14.7	18.4	5.2	8.6	6.8	0.5	2.2	11.6	21.9	2.2
	133.97		7.8	0.08	4.2	19.4	26.8	4.5	11.1	7.7	0.6	2.5	13.3	27.6	1.7
	135.58	-pyl	4.2	0.21	13.7	8.3	12.5	3.3	14.3	7.2	14.3	1.2	10.7	24.2	2.3
	136.15	-pyl	6.5	0.04	4.4	15.2	21.3	5.3	4.2	8.2	3.9	1.8	12.5	26.2	2.3
	136.67	-pyl	6.8	0.06	6.1	17.3	18.8	7.7	6.2	7.7	5.3	2.3	13.6	22.3	3.3
	136.94	-pyl	5.3	0.05	9.3	17.5	20.6	4.4	13.6	9.0	8.7	1.9	17.5	31.0	2.4
	137.31	-pyl	5.4	0.03	7.4	23.5	25.5	4.8	3.3		6.6		23.4	38.1	2.6
	137.68	-pyl	4.6	0.04	9.8	11.9	15.5	3.6	5.7	9.4	10.5	1.3	13.9	27.0	2.2
	137.96	-pyl	5.7	0.04	6.8	19.1	19.3	4.6	4.4	10.8	6.3	1.8	17.9	27.1	2.3
	138.38	-pyl	6.0	0.03	6.8	19.0	27.0	4.3	6.7	10.9	6.0	1.8	16.9	36.1	2.0
	138.74	-pyl	5.9	0.03	6.9	16.8	21.9	4.1					15.2	29.6	2.0
	139.01	-pyl	5.0	0.03	11.9	19.0	29.6	3.4	4.7	11.0	11.6	1.7	20.3	47.6	2.0
	139.65	-pyl	5.9	0.03	6.8	20.7	30.5	4.4	3.4	9.9		2.1	18.7	41.5	2.1
	139.71		5.1	0.01	23.9	9.9	12.8	2.2	2.4	5.5		1.8	10.4	20.2	1.3
	139.97	-pyl	6.6	0.02	4.7	25.0	36.1	4.3	3.0	12.1	5.4	2.1	20.2	43.7	1.9
	140.25	-pyl	6.0	0.02	6.1	22.6	38.4	3.4	3.3	12.4	6.9	1.8	20.1	51.1	1.6
	140.50	-pyl	6.2	0.01	4.5	29.1	33.8	3.1	9.3	15.3	5.1	1.9	25.3	44.1	1.4
	140.95	-pyl	6.0	0.02	5.3	30.5	41.5	3.7	4.1	16.1	6.3	1.9	27.3	55.6	1.8
	141.17	-pyl	6.3	0.02	5.8	20.4	30.6	5.2	3.4	12.6	6.6	1.6	17.4	39.0	2.4
	141.47	-pyl	6.4	0.02	5.2	21.9	31.6	3.2	7.4	13.0	5.3	1.7	18.3	39.6	1.4
	141.72	-pyl	6.7	0.02	4.9	18.6	26.3	4.5			5.2		14.9	31.4	1.9
	142.08	-pyl	6.5	0.01	4.3	19.1	26.7	4.1	3.9	11.6		1.6	15.7	33.0	1.8
	142.60	-pyl	4.5	0.01	3.4	13.5	13.8	2.6			3.7		16.0	24.6	1.7
	143.45	-pyl	3.7	0.05	7.9	41.4	37.1	2.5	9.6	13.1	7.7	3.2	59.4	79.9	1.9
	144.36		4.4	0.18	5.4	33.7	34.1	3.0	18.0	8.7	2.6	3.9	40.9	62.1	1.9
	145.61		6.1	0.04	5.1	40.1	36.3	4.8	13.5	13.4	2.0	3.0	35.3	47.9	2.3
	146.45		5.1	0.06	7.1	40.3	35.4	4.2	13.6	15.2	5.7	2.7	42.6	56.1	2.4
	147.30		5.8	0.04	4.5	27.1	25.5	6.3	10.1	12.6	2.3	2.2	25.0	35.3	3.1
	148.27		5.5	0.02	3.8	20.2	15.0	4.6	8.9	10.4	1.7	1.9	19.6	21.8	2.4
	149.30		7.1	0.02	4.3	37.1	37.9	5.2	9.8	12.1	3.7	3.1	27.9	42.9	2.1
	150.24		6.1	0.12	4.6	16.5	17.0	4.8	22.6	7.7	2.2	2.2	14.4	22.3	2.2
	152.08		5.7	0.03	2.7	7.3	10.0	4.1	17.8	5.7	1.5	1.3	6.9	14.2	2.1
	152.65		5.4	0.07	3.9	8.7	10.9	3.3	9.3	5.1	1.0	1.7	8.7	16.4	1.8
	153.18		6.4	0.02	2.7	6.7	6.6	3.4	9.1	4.0	0.6	1.7	5.7	8.3	1.5

Table S1 con't. Geochemical data for McRae Shale samples.

	depth (m)	Al wt %	Mn wt %	Fe wt %	Mo ppm	Re ppb	U ppm	Carbonate wt %	TOC wt %	S wt %	Mo/TOC ppm/wt%	Mo/Al ppm/wt%	Re/Al ppb/wt%	U/Al ppm/wt%
ave upper crust*		8.04	0.06	3.5	1.50	1.00**	2.80					0.19	0.12	0.35
												Enrichment Factor	Enrichment Factor	Enrichment Factor
	154.43	7.1	0.02	6.8	6.7	8.2	4.5	15.0	4.1	2.5	1.6	5.1	9.3	1.8
	156.05	7.4	0.03	3.3	7.4	10.7	4.8	11.0	4.8	0.3	1.6	5.4	11.7	1.9
	157.80	7.2	0.08	8.0	8.0	10.2	4.7	24.3	4.3	2.4	1.9	6.0	11.5	1.9
	158.91	7.3	0.04	5.9	6.1	7.6	4.5	15.9	4.8	1.6	1.3	4.4	8.3	1.8
Siderite BIF	161.32	7.0	0.10	8.7	4.9	10.8	4.9	22.6	5.8	1.6	0.8	3.7	12.4	2.0
	162.80	5.4	0.21	18.9	4.0	4.7	3.3	51.0	3.3		1.2	4.0	7.1	1.7
	163.95	5.6	0.18	20.1	5.1	6.5	3.0	52.4	3.2	2.2	1.6	4.8	9.3	1.5
	165.56	3.6	0.29	18.1	3.3	5.5	2.2	52.1	2.9	0.8	1.2	4.9	12.4	1.8
	167.76	2.6	0.37	15.0	1.4	2.4	1.8	44.4	1.8	0.5	0.8	3.0	7.3	2.0
	168.36	3.1	0.40	16.0	3.3	3.2	2.0	45.4	1.9	0.9	1.8	5.7	8.1	1.8
	168.90	2.2	0.49	19.7	1.2	2.1	1.3	52.1	1.9	2.4	0.6	3.0	7.9	1.7
	169.28	4.5	0.30	13.5	2.0	4.7	3.8	32.9	2.7	1.5	0.8	2.5	8.4	2.5
	169.47	2.8	0.29	19.8	2.4	3.3	1.8	43.6	2.0	9.1	1.2	4.6	9.4	1.8
	169.68	3.5	0.27	12.8	1.8	2.6	1.8	50.7	2.0	1.5	0.9	2.8	6.0	1.5
	169.94	1.6	0.54	21.2	1.4	1.6	1.0	39.3	2.5	3.5	0.6	4.6	8.0	1.8
	170.17	3.8	0.37	15.7	2.1	3.2	2.9	50.5	2.1	2.4	1.0	2.9	6.7	2.2
	170.39	2.8	0.48	18.5	1.6	2.8	1.7	48.8	2.4	3.1	0.7	3.0	8.0	1.8
	170.55	3.6	0.39	16.2	2.2	4.3	2.6	27.2	3.1	2.6	0.7	3.3	9.6	2.0
	170.86	4.4	0.33	13.7	1.9	3.8	3.6	41.1	2.2	1.8	0.9	2.3	7.0	2.4
	170.94	3.5	0.35	16.6	2.0	3.5	2.2	28.0	3.0	5.4	0.7	3.1	8.0	1.8
	171.22	4.4	0.27	13.8	2.9	4.1	3.4	26.6	2.8	3.2	1.0	3.5	7.4	2.2
S2	173.09	5.5	0.16	13.0	3.4	4.0	3.3	31.5	3.1	1.7	1.1	3.3	5.8	1.7
	173.50	5.6	0.26	13.9	3.0	4.8	3.7	36.4	2.7	4.4	1.1	2.9	6.9	1.9
	173.73	4.0	0.42	16.8	2.5	4.5	2.0	42.0	2.8	2.2	0.9	3.3	9.1	1.5
	174.67	1.9	0.14	4.8	0.9	1.3	1.0	33.0	2.9	3.2	0.3	2.6	5.3	1.5
	175.51	5.9	0.20	9.2	3.3	6.1	4.3	23.8	3.8	2.4	0.9	3.0	8.3	2.1
	177.10	6.5	0.16	8.8	3.1	8.7	4.6	20.0	5.0	3.0	0.6	2.6	10.8	2.1
	178.61	6.3	0.16	7.3	3.2	7.4	3.7	15.2	4.9	3.5	0.7	2.7	9.4	1.7
	178.83	6.2	0.12	5.2	3.4	10.1	3.1	16.6	6.3		0.5	2.9	13.0	1.4
	179.05	6.2	0.17	7.6	3.0	7.9	3.9	15.9	4.7	3.1	0.6	2.6	10.2	1.8
	180.33	5.2	0.25	9.3	2.9	7.9	2.8	19.9	5.0	3.4	0.6	3.1	12.3	1.6
	181.20	4.8	0.32	10.1	2.0	9.3	3.0	23.8	4.2	2.7	0.5	2.3	15.8	1.8
	182.50	5.4	0.09	5.1	2.5	4.3	3.0	14.1	4.4	1.4	0.6	2.5	6.4	1.6
	183.65	4.8	0.44	8.0	2.4	4.1	2.9	22.2	3.1	2.1	0.8	2.7	7.0	1.8
	185.43	3.4	0.56	10.2	1.8	2.9	2.2	34.1	2.5	1.2	0.7	2.8	6.8	1.8
	187.46	6.0	0.10	5.7	3.2	5.0	4.2	13.7	3.6	1.5	0.9	2.9	6.8	2.0
	188.01	5.5	0.18	6.7	4.6	8.2	3.6	17.1	4.0	3.0	1.2	4.5	12.1	1.9
	188.87	4.9	0.19	7.0	7.7	5.3	3.5	22.7	3.3	1.5	2.3	8.5	8.8	2.0
	189.39	4.8	0.30	6.7	3.6	11.8	3.9					4.0	19.6	2.3

* Average upper crust data from Taylor and McClennan (1985); **average [Re] from Selby et al., (2007).

Table S3. Re-Os data for Mt. McRae Shale samples.

Re-Os abundance and isotope data for the Mt. McRae Shale, western Australia

Sample	Re (ppb)	Os (ppt)	^{192}Os (ppt)	$^{187}Re/^{188}Os$	$^{187}Os/^{188}Os$	rho
ABDP9-128.71	11.59	628.8	133.2	173.11 (1.42)	7.3989 (0.0675)	0.717
ABDP9-128.84	11.49	513.8	86.1	265.57 (3.12)	11.3592 (0.1463)	0.822
ABDP9-129.15	13.32	467.3	47.4	558.35 (10.44)	23.6301 (0.4745)	0.895
ABDP9-129.36	20.94	792.7	96.8	430.21 (4.44)	18.3693 (0.1997)	0.830
ABDP9-129.85	21.04	761.0	83.4	501.84 (5.43)	21.3396 (0.2533)	0.808
ABDP9-145.22	39.06	1148.2	44.6	1742.85 (23.25)	73.9781 (1.0922)	0.836
ABDP9-146.08	27.20	820.3	39.2	1381.41 (19.89)	58.7478 (0.8446)	0.937
ABDP9-147.10	28.60	911.3	58.8	967.45 (10.94)	41.5033 (0.5201)	0.809
ABDP9-148.32	21.94	681.0	39.2	1113.77 (16.10)	47.4586 (0.6796)	0.945

Note: Numbers in parentheses denote measured 2σ uncertainty in the $^{187}Re/^{188}Os$ and $^{187}Os/^{188}Os$ isotope ratios as determined by numerical error propagation.

Total procedural blanks for Re and Os were 9.5 $\pm$ 0.3 pg and 0.39 $\pm$ 0.25 pg, respectively. $^{187}Os/^{188}Os$ of 0.224 $\pm$ 0.068 (1σ, n=4).

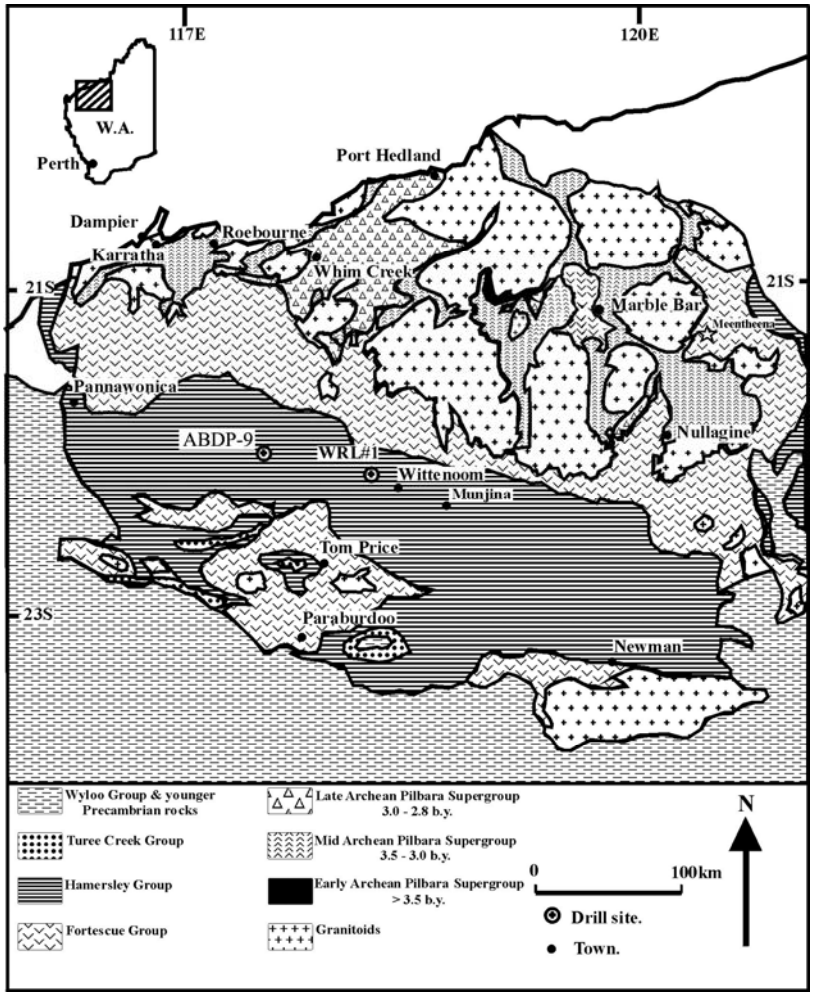

Figure S1. Simplified geologic map of the Pilbara Craton showing location of the ABDP-9 drill site.

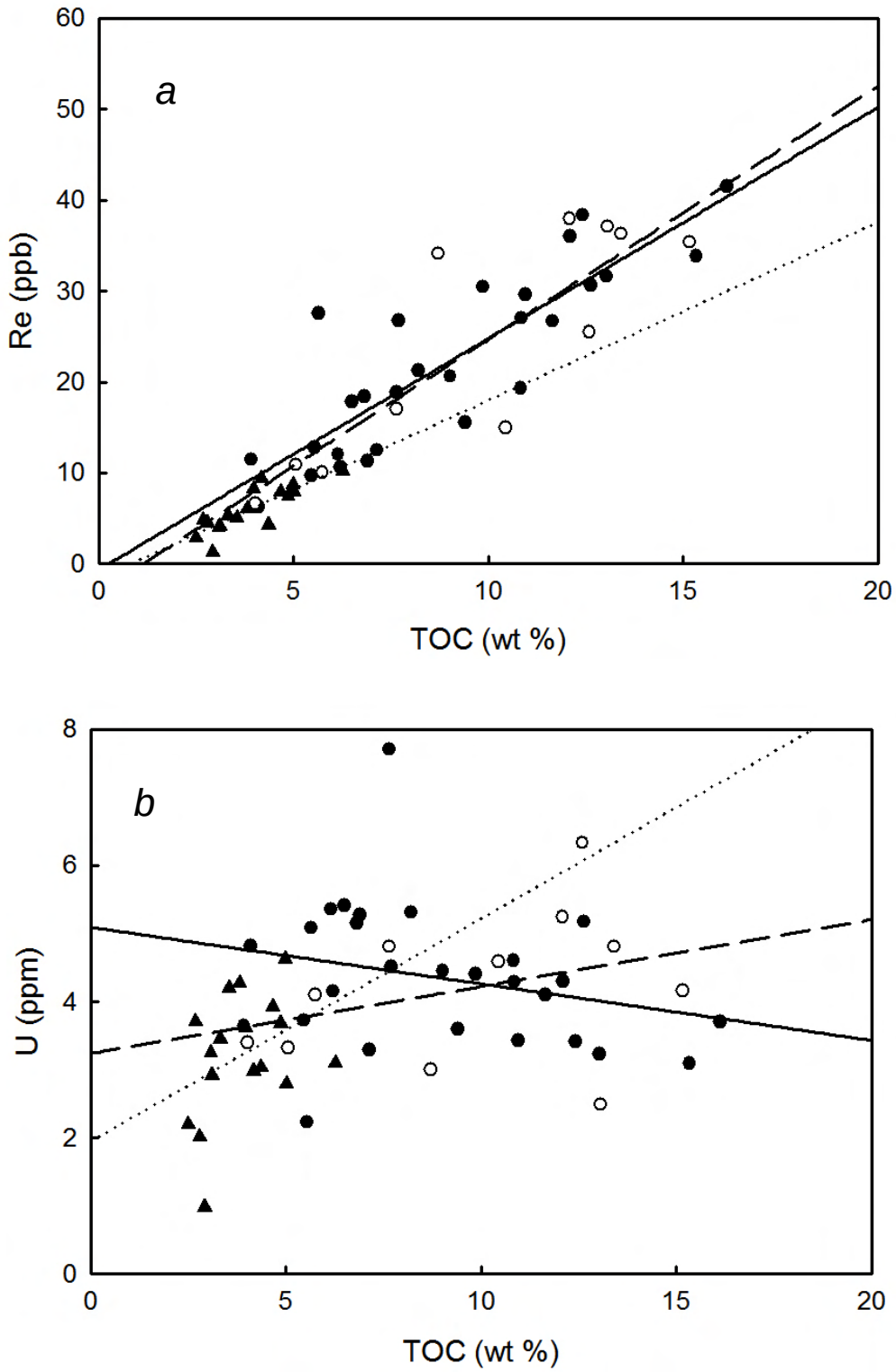

Figure S2. Relationship between (a) Re and TOC and (b) U and TOC in organic carbon-rich, pyritic intervals in the Mt. McRae Shale. Circles are from interval S1 (125.5 – 153.3 m). The metal-enriched zone of S1 below 143 m (open circles) is differentiated from the upper zone, (solid circles). Triangles are from interval S2 (173.0 – 189.7 m).

References

1. H. Ohmoto, Y. Watanabe, H. Ikemi, S. R. Poulson, B. E. Taylor, *Nature* **442**, 908 (2006).
2. R. A. Creaser, P. Sannigrahi, T. Chacko, D. Selby, *Geochim. Cosmochim. Acta* **66**, 3441 (2002).
3. D. Selby, R. A. Creaser, *Chem. Geol.* **200**, 225 (2003).
4. B. S. Kendall, R. A. Creaser, G. M. Ross, D. Selby, *Earth Planet. Sci. Lett.* **222**, 729 (2004).
5. K. Ludwig, *User's manual for Isoplot/Ex rev. 3.00: A Geochronological Toolkit for Microsoft Excel*, Special Publication 4 (Berkeley Geochronology Center, Berkeley, 2003), pp. 70.
6. M. I. Smoliar, R. J. Walker, J. W. Morgan, *Science* **271**, 1099 (1996).
7. D. Selby, R. A. Creaser, *Geology* **33**, 545 (2005).
8. D. Selby, R. A. Creaser, M. G. Fowler, *Geochim. Cosmochim. Acta* **71**, 378 (2007).
9. B. K. Esser, K. K. Turekian, *Geochim. Cosmochim. Acta* **57**, 3093 (1993).
10. B. Peucker-Ehrenbrink, B. M. Jahn, *Geochem. Geophy. Geosys.* **2** (2001).
11. Y. Hattori, K. Suzuki, M. Honda, H. Shimizu, *Geochim. Cosmochim. Acta* **67**, 1195 (2003).
12. W. D. Sun, V. C. Bennett, S. M. Eggins, V. S. Kamenetsky, R. J. Arculus, *Nature* **422**, 294 (2003).
13. B. Peucker-Ehrenbrink, *Geochim. Cosmochim. Acta* **60**, 3187 (1996).
14. G. Ravizza, K. K. Turekian, *Earth Planet. Sci. Lett.* **110**, 1 (1992).
15. R. Oxburgh, *Earth Planet. Sci. Lett.* **159**, 183 (1998).
16. S. Levasseur, J. L. Birck, C. J. Allegre, *Earth Planet. Sci. Lett.* **174**, 7 (1999).
17. B. S. Kendall, R. A. Creaser, paper presented at the Sixteenth Annual V. M. Goldschmidt Conference, Melbourne, Australia, 27 Aug to 1 Sep 2006.
18. T. Meisel, R. J. Walker, A. J. Irving, J. P. Lorand, *Geochim. Cosmochim. Acta* **65**, 1311 (2001).
19. R. J. Walker *et al.*, *Geochim. Cosmochim. Acta* **66**, 4187 (2002).
20. R. J. Walker, H. M. Prichard, A. Ishiwatari, M. Pimentel, *Geochim. Cosmochim. Acta* **66**, 329 (2002).
21. M. Sharma, G. J. Wasserburg, A. W. Hofmann, D. A. Butterfield, *Earth Planet. Sci. Lett.* **179**, 139 (2000).
22. R. R. Cave, G. E. Ravizza, C. R. German, J. Thomson, R. W. Nesbitt, *Earth Planet. Sci. Lett.* **210**, 65 (2003).
23. C. E. Martin, B. Peucker-Ehrenbrink, G. J. Brunskill, R. Szymczak, *Earth Planet. Sci. Lett.* **183**, 261 (2000).
24. K. Yamaguchi, thesis, Pennsylvania State University (2002).
25. C. Scott, paper presented at the 2006 Annual Meeting of the Geologic Society of America, 22 October 2006.